Flow Mechanics of Rock Avalanches

Geology Department
University of Maryland
College Park, MD

Submitted by:

Jeff Harp
Geology 394
University of Maryland, College Park, MD
November 25, 2002

Advisor:
Dr. Julio Friedmann

Abstract

Although rock avalanches are dangerous infrequent events, they are not well understood. A good way to understand how rock avalanches flow, is to model them experimentally. By simulating rock avalanches on a scaled-down model apparatus, flow character and morphology can be observed. By changing experimental parameters such as substrate and material, comparisons can be made as to how they affect the flow character. Morphology of rock avalanches seems to be influenced by substrate as seen in Blackhawk and Sherman Glacier rock avalanches.

In this study, two different substrates were used (smooth and rough) along with three different flow materials, to determine the importance of the coefficient of friction. Two different views of the flow were studied for the experiment, a side view at the base of the flow where the material makes contact with the substrate, and at the top of the flow where the material runs out. It was shown at the base of the flow of the smooth surface, the smallest material (fine sand) had the highest velocity. At the top of the flow of the smooth surface, the lighter material (rubber track) had higher velocity and longer run-out. It was shown at the base of the flow of the rough surface, that all material slowed down significantly due to the increased friction. At the top of the flow of the rough surface the smallest material (fine sand) had the highest velocity and covered the largest area. The overall morphologies of these dry granular materials have parabolic shapes similar to that of the Blackhawk type rock-avalanches.

Table of Contents

List of Tables

List of Figures

I. Introduction/Background

Rock avalanches are a rare class of landslide, but are large in scope. Compared to other natural disasters (landslides, floods), rock avalanches occur with larger volumes, speeds and destruction. Because of their high mobility and long run-outs, they are extremely dangerous. The Transportation Research Boards, Commission on Sociotechnical Systems estimates that the cost of damage caused by slope failures in the United States exceeds one billion dollars annually. The Federal Highway Administration reports spending 50 million dollars a year to repair damage done to the National Highway System due to major landslides (Schuster et al., 1978). Not only is there damage caused by landslides and rock avalanches, but also many lives have been lost to these infrequent, but potentially catastrophic events. In fact, David Keefer (1984) wrote, "Rock avalanches are among the most dangerous landslides triggered by seismic events . . . they have killed more people than any other type of landslide in recent earthquakes."

Table 1 shows the location, date, run-out, volume and deaths caused by some rock avalanches.

Table 1. Location, date, run-out, volume and deaths caused by rock avalanches [a]

Name/Location	Date	Run-Out (meters)	Volume (m^3)	Deaths
Elm/Switzerland	1882	1,500	10 Million	115
Huascaran/Peru	1970	14,500	80 Million	18,000
Mantaro/Peru	1964	31,000	1.6 Billion	5,000
Vaiont/Italy	1963	2,000	250 Million	3,000
Frank/Alberta	1903	----------	30 Million	70
Madison Canyon/ Montana	1959	----------	28 Million	26
Sherman/Alaska	1964	3,000	30 Million	--------
Black Hawk/ California	Prehistoric	8,000	283 Million	--------
Tsiolkovsky/ Moon	----------	50,000	$1.2x10^{12}$	--------
Buller River/ New Zealand	1968	----------	---------	--------
Mt. Baldwin/ California	1980	----------	--------	---------
Khait/ Soviet Union	1949	----------	---------	12,000
Silver Reef/ California	------	----------	220 million	---------

[a] (Keefer, 1984; Schuster et al., 1978; Shreve, 1968; Heim, 1882; Hsu, 1975)

There are certain identifying features associated with rock avalanches. Some of these include:

1. Brecciation
2. Preserved Inherited Stratigraphy
3. Injected Dikes
4. Small Mixed Basal Zone
5. Long Run-Out

Normal run-out for landslides have a ratio of approximately 1:1 height vs. distance traveled, but rock avalanches travel out 1:20 or greater (Yarnold, 1993; Friedmann, 1997). These features, and the understanding that rock avalanches only occur

on slopes higher than 150 m with an inclination angle greater than 25 degrees (Keefer, 1984), can be used to identify susceptible source areas. One could better understand how and where rock avalanches are most likely to occur with the knowledge of how they flow.

Earthquakes mainly initiate rock avalanches, although they can be expedited by the undercutting of their slopes by mining, as well as by fluvial and glacial erosion (Keefer, 1984). Two types of rock-avalanches initiated by earthquakes are the Blackhawk and Sherman Glacier landslides. Since rock avalanches are so devastating, it is important to understand them.

There are two main types of rock avalanches that I am concerned with:

1. Sherman Glacier Type
2. Blackhawk Type

Sherman Glacier type rock avalanches (shown in Fig. 1) are named after the Sherman glacier landslide in Alaska in 1964, which was initiated by a magnitude 9.0-earthquake. This event fell 600 meters and flowed out 3 miles, creating a deposit 3-6 meters thick at high speeds (Dutch, 1999). There are certain features associated with it: longitudinal ridges, which run parallel to flow direction, a tapered snout, and digitate toe. These features are thought to be related to transport over icy substrates.

Blackhawk type avalanches (shown in Fig. 2) are named after the Blackhawk landslide in Lucerne Valley, Southern California, which occurred approximately 15-17,000 years ago. It had a total volume of 283 million cubic meters of rock. This massive landslide flowed five miles in length and two miles in width at incredibly fast speeds (approximately 200mph), creating a deposit 30 to 100 feet thick over the terrain

(Shreve, 1968). There are specific features associated with it: transverse ridges, which run perpendicular to flow direction, and raised ridges, especially at the edges of the flow. These features are typical of rock avalanches that occur in dry areas. By their associated features, these two types of rock avalanches depict distinctly different morphology.

Fig. 1. Sherman Glacier Landslide. A 1964 Alaskan earthquake Initiated this landslide, which flowed 3 km out over ice. Note the longitudinal ridges, digitate and tapered toe. (Http://www.ireap.umd.edu/granular/)

Fig. 2. Blackhawk landslide. A prehistoric California landslide initiated by seismic activity. Note the transverse ridges and raised rim. (Http://www.ireap.umd.edu/granular/)

Currently there are different views on the flow mechanics of rock avalanches. Shreve (1968) believes that the long run-out rock avalanches are able to travel long distances by riding atop a cushion of compressed air. The trapped air creates a low frictional basal layer, allowing the long run-out. Other views of the long run-out

phenomena include Kent's (1966) partially fluidized material, Campbell et al's (1995) self-lubrication theory, and the idea of partial melting caused by frictional heating during emplacement (Erismann, 1979). In rock-avalanche systems, it has been shown that the larger the volume of the slide, the smaller the frictional resistance (Hsu, 1975). Campbell et al., (1995) states; "there must, indeed, be some mechanism that reduces the friction as the slide volume is increased."

The tangent of the internal angle of friction (H/L) is the ratio of the drop distance (initial) to the farthest resting point of the flow (travel distance) (Shreve, 1968). This internal angle of friction is sometimes referred to by the name "Fahrboschung" and is independent of the individual material friction characteristics. The idea that different substrate friction coefficients can create different flow characteristics, which can link morphology to substrate, seems quite possible. The Blackhawk and Sherman Glacier avalanches are good examples of events that traversed different substrates producing different morphologies.

The mechanics for long run-out rock avalanches are still unknown, but many think that it has to do with frictional character at the base of the flow. Flow character of model rock avalanches can be modified by changing the frictional qualities of the substrate. With increasingly better models, more information will be observed, which creates a better understanding of the key parameters that control the flow process, including velocities and final morphology. With an understanding of the flow characteristics, the ability to properly identify a rock-avalanche hazard might be possible, enabling mitigation of some catastrophic events.

The research I conducted is experimental and is related to the flow character of rock avalanches. I think these morphologies are developed by the different characteristics imposed upon them by the material and its substrate. Different substrates create different shears, which create different flow morphologies. This leads to my hypothesis:

The substrate (coefficient of friction) is a critical parameter in the flow mechanics (as measured by velocity, thickness and distance) of dry granular landslides.

II. Method of Analysis

Some model rock-avalanche experiments have been performed on flow mechanics. Campbell et al. (1995) produced computer simulations of rock avalanches using two-dimensional disk shaped objects. Hsu (1975) produced simulations of rock avalanches using a bentonite fluid model. Both models indicate that increasing the slide volume will decrease the basal friction coefficient. The model that I used is focused on the flow mechanics of *three dimensional, dry* granular materials.

Dr. Wolfgang Losert and Mr. Don Martin of the University of Maryland Physics Department created a model rock avalanche apparatus (Fig. 3), located in the Pattern Formation and Granular Dynamics Laboratory in the Energy Research Building at the University of Maryland (http://www.ipr.umd.edu/granular/). Dr. Wolfgang Losert is the Principal Investigator in charge of the Granular Dynamics laboratory. He and his students (Dominic Britti, Kyuyong Lee, Masahiro Toiya and Saunder Van de Meer) assisted me with the understanding of the particle tracking software, fast camera and

high-resolution camera. Dr. Julio Friedmann has been critical in the understanding of granular flow material, as well as the overall understanding of rock avalanches.

A. Apparatus

The rock avalanche apparatus (Fig. 3) was built with the dimensions of:

- Slope area: 28 x 29 cm
- Run-out area: 89 x 155 cm
- Angle of slope: 33 degrees

Fig 3. Experimental Rock Avalanche Apparatus

The apparatus itself was built from a mixture of wood, plexiglas and aluminum. With the help of Don Martin, we designed and I built the support arms that attach the avalanche apparatus to a high frequency waveform generator.

The rock-avalanche apparatus is scaled to simulate actual rock avalanches. By scaling down the material 3 orders of magnitude, a 500-μm grain of sand represents a 0.5-meter clast of rock. A seismic shock producing an earthquake frequency was scaled up to produce 60 Hz for the Experiment. The other factors in the experiment were scaled

down 3 orders of magnitude as well. By scaling the model, a manageable apparatus was created.

Our experiment begins by setting up the rock avalanche apparatus. This apparatus is attached to a high frequency waveform generator. A fast camera is placed normal to the slope on the apparatus and is focused through the clear Plexiglas. A high-resolution camera is placed above the run-out area, close to normal to the apparatus. Once the cameras are in place, the high frequency waveform generator is set to shake at a frequency of 60 Hz with amplitude of 3.5V. The dislodging of the material represents the failure produced from an earthquake that would initiate a true rock avalanche. As the material reaches failure and begins to dislodge, the cameras photograph the particles as the material flows. The apparatus shakes for a total time of 20 seconds.

After the particles were photographed, they were downloaded into a computer and processed with the help of some particle-tracking programs (IDL, Scion Image, and Igor). The particle tracking program works by user defined parameters. Three runs were performed in order to obtain an average for each parameter. These parameters for the particle tracking software seem to work the best for tracking sand grains, although they did vary. These are located in Table 2.

Table 2. Definitions and Values of Parameters used in Particle Tracking software

Parameter	Definition	Typical values
Bandpass	The maximum and minimum wavelength of the bandpass filter	1(min), 8(max)
Threshold	Brightness of the particles to be tracked	20
Feature 1	Diameter used for finding the centroid of a bright spot	13
Feature 2	Separation between bright spots	15
Delta Cut	Number of pixels on the fringe that will be ignored	10
Delta Max	Maximum displacement between frames	10
Goodenough	Number of frames to track an individual particle	30
Steps Memory	How often a particle can be lost and found	3

B. Parameters

The model avalanche apparatus allowed me to change and measure different parameters associated with the flow mechanics of granular material. The parameters include:

1. Type of particles
2. Substrate
3. Size of particles
4. Thickness

In order to obtain varying frictional conditions, two substrates were used, smooth Plexiglas and wire mesh (rough). Other substrates were used (Styrofoam and sand paper), but proved to be unsuitable due to increased static charge. Three different sized flow materials were used. These included sub-rounded very fine sand grains,

approximately 100µm, sub-rounded coarse sand grains 2mm, and a sub-angular rubber material 0.5mm used on athletic tracks. The lightest is the rubber track material.

C. Calibration of Equipment and Standards

The high-frequency waveform generator (Agilent 33120A, 15 MHz function/arbitrary waveform generator) can produce many different types of waves (sine, square etc.) as well as frequencies (1-15MHz). The waveform generator has been calibrated to the below stated specification: For a sine wave of 50.00 Ω's, 3.50 Volts (amplitude) and a frequency of 1.00kHz, the fluctuation for ohms is ± 0.1, frequency is ± 0.01, and the amplitude is ± 0.0035 Volts.

The particle tracking software is capable of measuring many different parameters including brightness, width of particle to be tracked, and how long to track the particle, all of which are user defined. The uncertainty of the particle tracking software is one pixel.

The photron fastcam super 10Kc model 10000 is capable of imaging up to 3000 frames/sec. I used this camera to photograph particles at 1000 frames/sec. There is no error associated with the actual number of frames produced. The time error associated with the individual frames photographed 1/1000 of a second is so minimal that it is not calculated. The high-resolution camera will photograph 8.07 frames per second; this camera also has negligible error associated with it.

III. Presentation of Data

A total of thirty-six runs were performed using the above-mentioned apparatus to produce the observations stated. These consisted of 18 runs utilizing the fast-camera, and 18 runs using the high-resolution camera. Two different substrates were used:

1. Smooth substrate (Plexiglas)
2. Rough substrate (wire mesh 0.1cm spacing)

Table 3. Type of Experiments performed.

Number of Runs	Frequency/Amplitude	Camera	Flow Material	Substrate
3	60 Hz/3.5V	FC/HR	Fine sand (100μm)	Smooth
3	60 Hz/3.5V	FC/HR	Coarse sand (2mm)	Smooth
3	60 Hz/3.5V	FC/HR	Track material (0.5mm)	Smooth
3	60 Hz/3.5V	FC/HR	Fine sand (100μm)	Rough
3	60 Hz/3.5V	FC/HR	Coarse sand (2mm)	Rough
3	60 Hz/3.5V	FC/HR	Track material (0.5mm)	Rough

The shaking frequency and amplitude were set at 60 Hz and 3.5V for all runs. These runs were repeated 3 times for reproducibility and to obtain an average.

The graphs are different plots, created from data obtained by particle tracking the material. These graphs enabled me to compare the changing velocities of the flow front

as well as at the flow bottom, distance versus time, front center of flow and front area with regard to the changing substrate, and material.

Figure 4 shows the averaged mean velocity of the flow materials over the smooth substrate. The results show that all three materials were the slowest at the contact with the substrate. The fine sand has the highest velocity while the track material was the slowest with nearly zero velocity. The coarse sand maintained a slow steady velocity throughout the thickness of the flow.

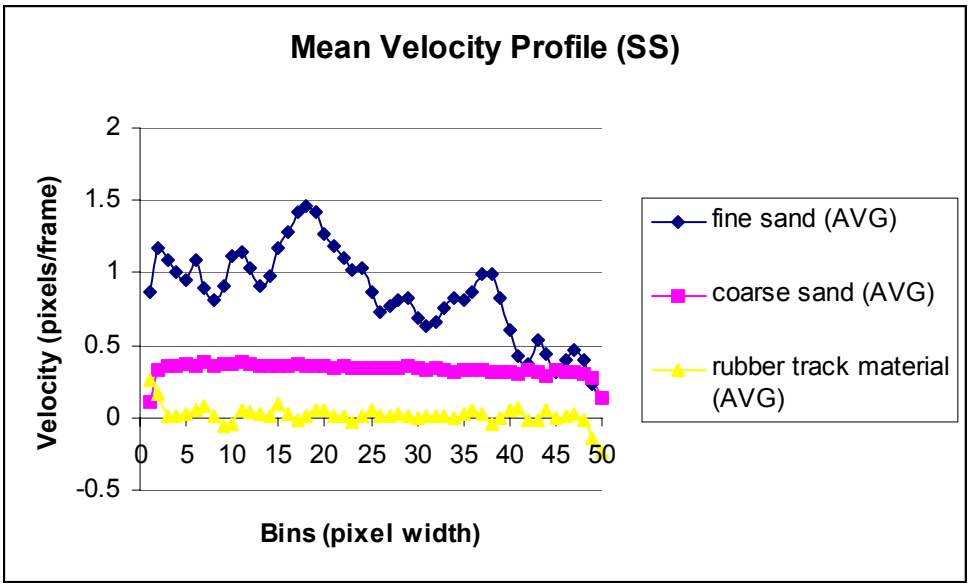

Fig 4. Flow Direction Mean Velocity for the viewing area of the fast-camera. The total distance from the top of flow located at (0 bins), to the bottom of flow located at (50 bins) is 0.5 cm. Each bin is 5 pixels wide. The fifty bins are parallel to slope surface, which is at an angle of 33°. Note that the velocity decreases slightly as the flow gets closer to the substrate. Uncertainty is ± 1 pixel and displayed in 1 σ.

Figures 5a-c show the velocity of the flow fronts (in the direction of flow) for each material on the smooth substrate.

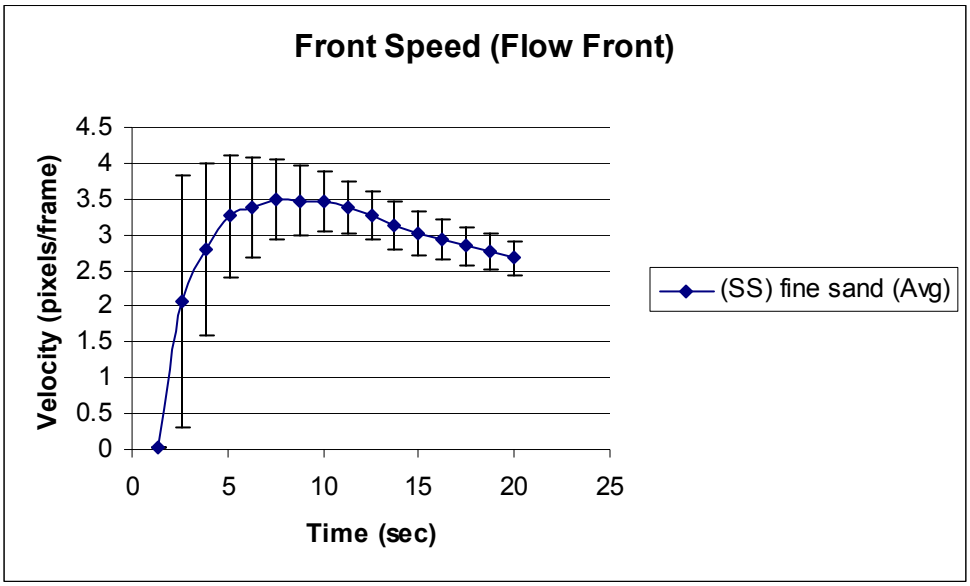

Fig 5a. Velocity of Flow Front (in Direction of Flow). Note the tapering slope beginning at 20 sec. The run consisted of fine sand with a thickness of 10 cm over smooth substrate. The range for the high-resolution camera is ± 1 pixel and displayed 1 σ.

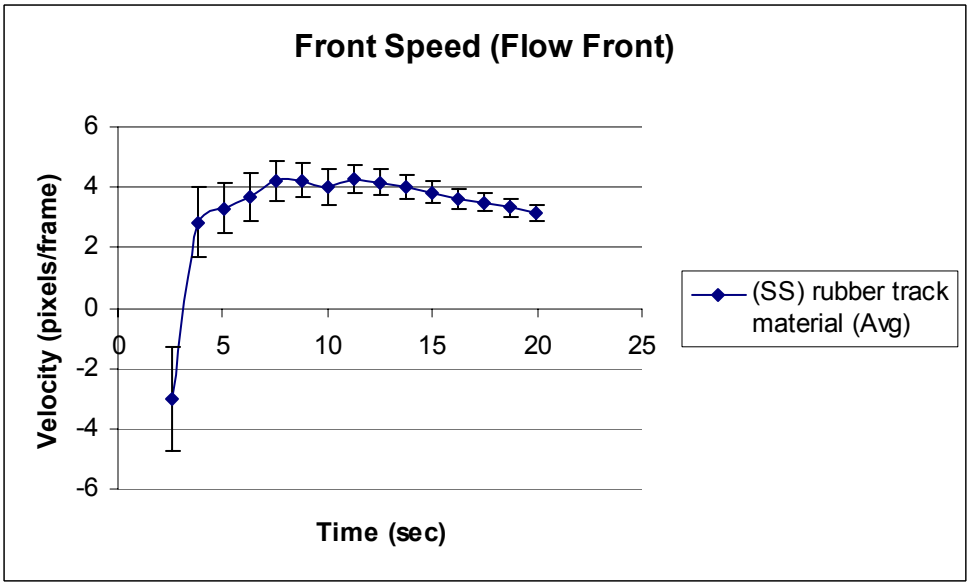

Fig 5b. Velocity of Flow Front (in Direction of Flow). The run consisted of rubber track material with a thickness of 10 cm over smooth substrate. The range for the high-resolution camera is ± 1 pixel and displayed 1 σ.

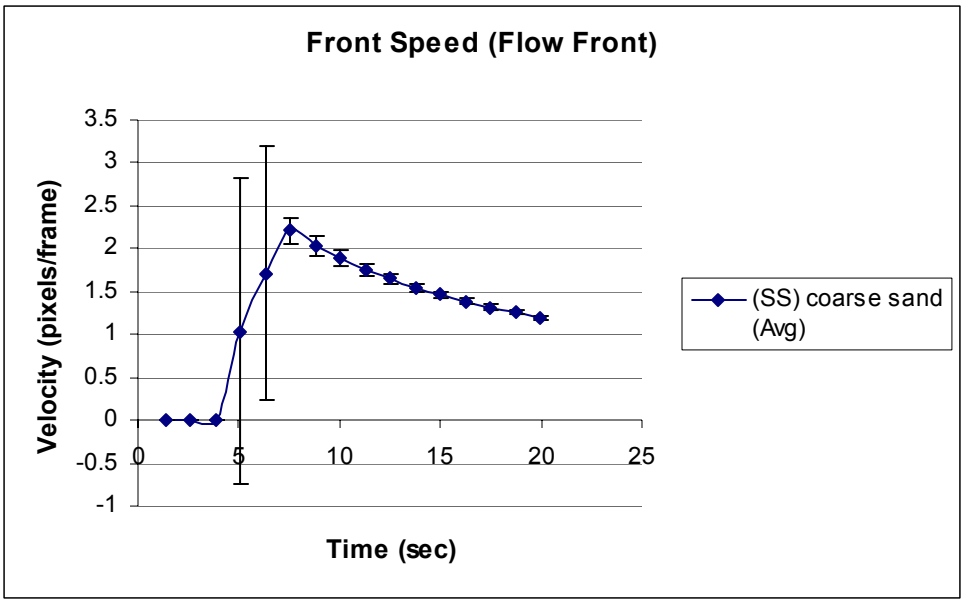

Fig 5c. Velocity of Flow Front (in Direction of Flow). The run consisted of coarse sand material with a thickness of 10 cm over smooth substrate. The range for the high-resolution camera is ± 1 pixel and displayed 1 σ.

Figures 6a-c show distance vs. time plots of the front center of flow of each material on the smooth substrate.

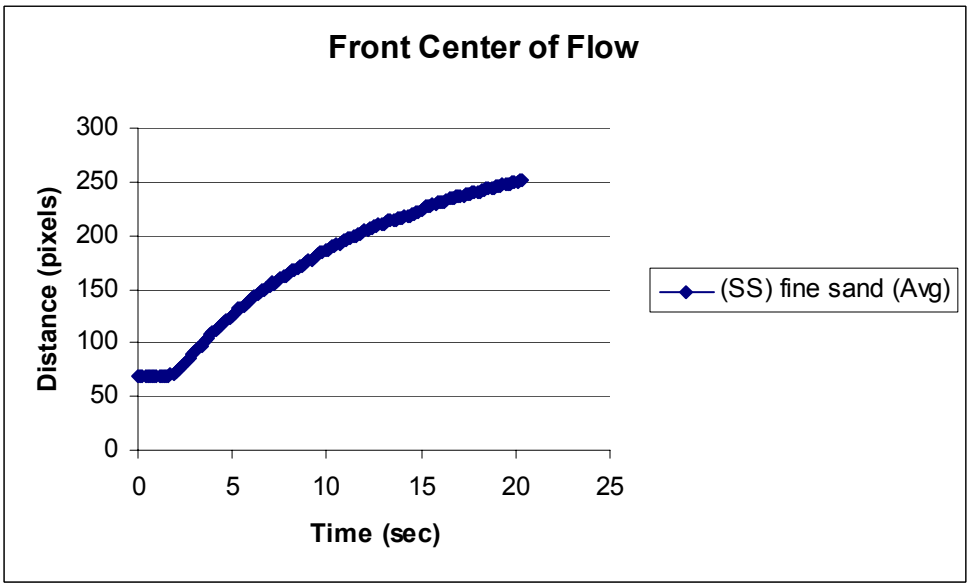

Fig 6a. Velocity of Front center of flow Front (in Direction of Flow). The run consisted of fine sand material with a thickness of 10 cm over smooth substrate. The uncertainty for the high-resolution camera is ± 1 pixel and displayed 1 σ. The front center of the flow is almost linear with respect to distance.

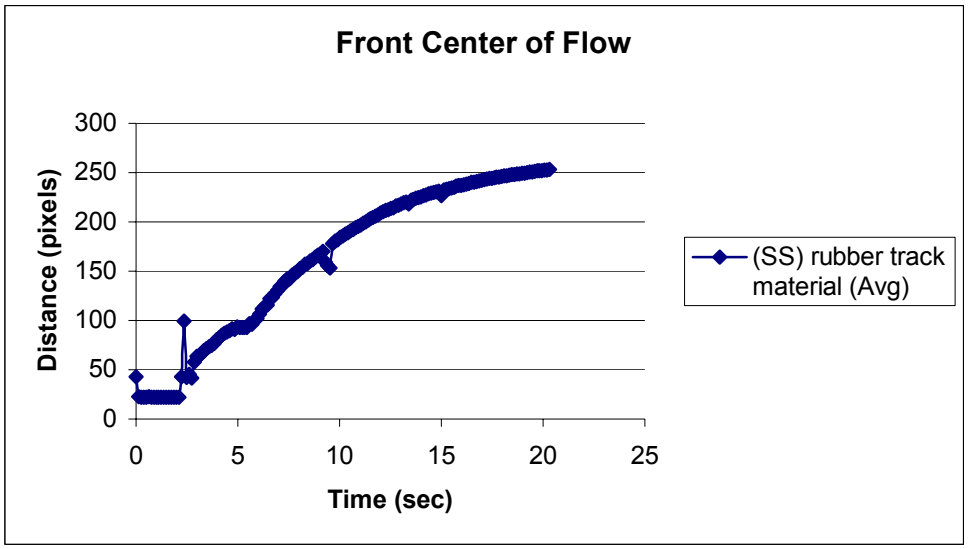

Fig 6b. Velocity of Front center of flow Front (in Direction of Flow). The run consisted of rubber track material with a thickness of 10 cm over smooth substrate. The uncertainty for the high-resolution camera is ± 1 pixel and displayed 1 σ.

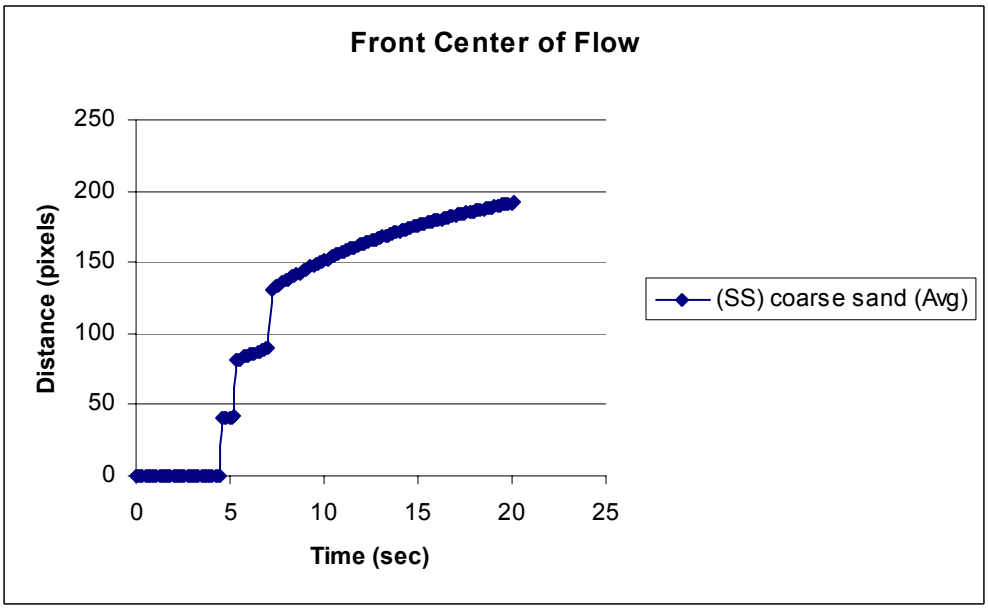

Fig 6c. Velocity of Front center of flow Front (in Direction of Flow). The run consisted of coarse sand material with a thickness of 10 cm over smooth substrate. The uncertainty for the high-resolution camera is ± 1 pixel and displayed 1 σ. The particle tracking software had difficulty tracking the first part of the coarse sand experiment for all three runs, which resulted in loss of data at the beginning.

Figures 7a-c show the front area of flow for all materials on the smooth substrate.

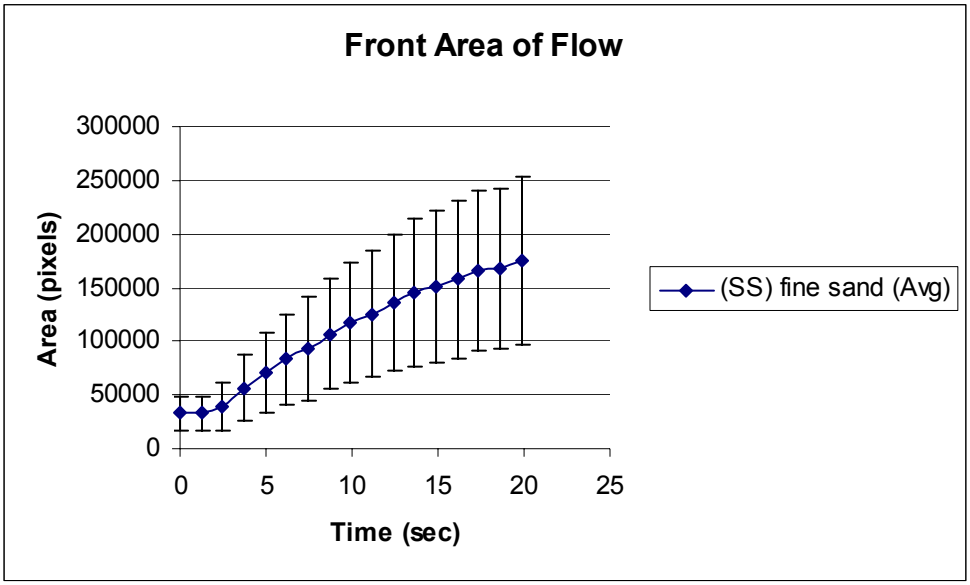

Fig 7a. The Front area of flow Front (in Direction of Flow). The run consisted of fine sand material with a thickness of 10 cm over smooth substrate. The range for the high-resolution camera is ± 1 pixel and displayed 1 σ.

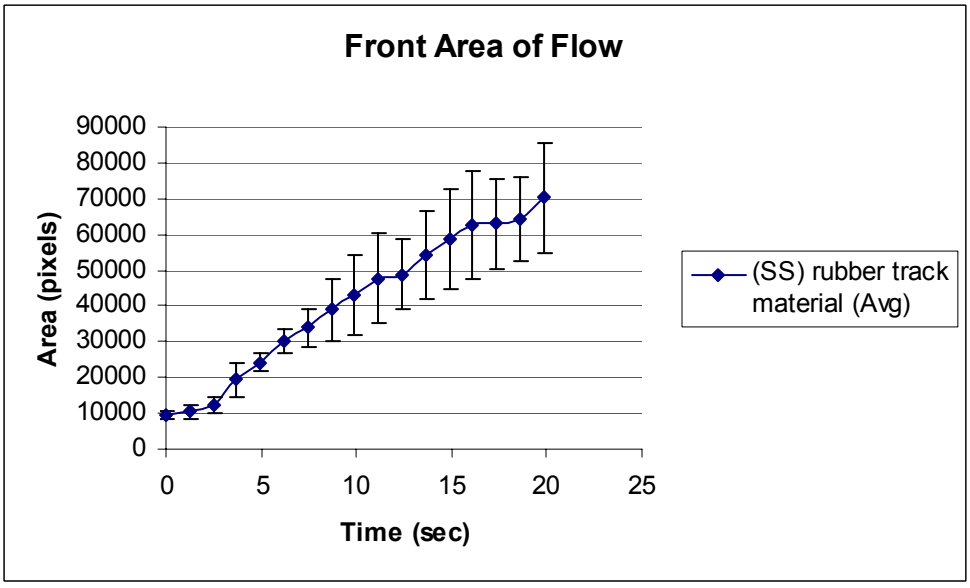

Fig 7b. Velocity of Front area of flow Front (in Direction of Flow). The run consisted of rubber track material with a thickness of 10 cm over smooth substrate. The range for the high-resolution camera is ± 1 pixel and displayed 1 σ.

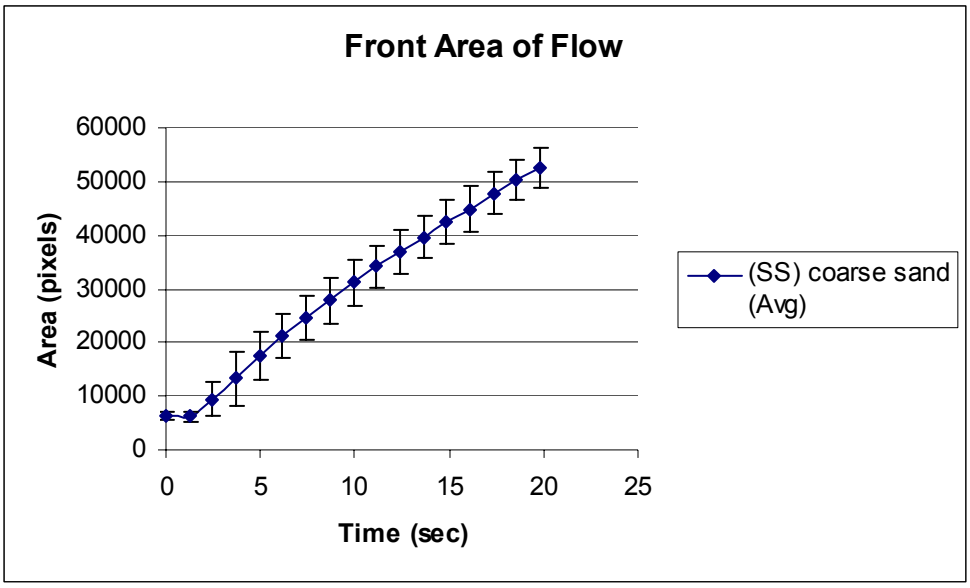

Fig 7c. Velocity of Front area of flow Front (in Direction of Flow). The run consisted of coarse sand material with a thickness of 10 cm over smooth substrate. The range for the high-resolution and camera is ± 1 pixel and displayed 1 σ.

Figures 8a-c show position overlays of each material on the smooth substrate.

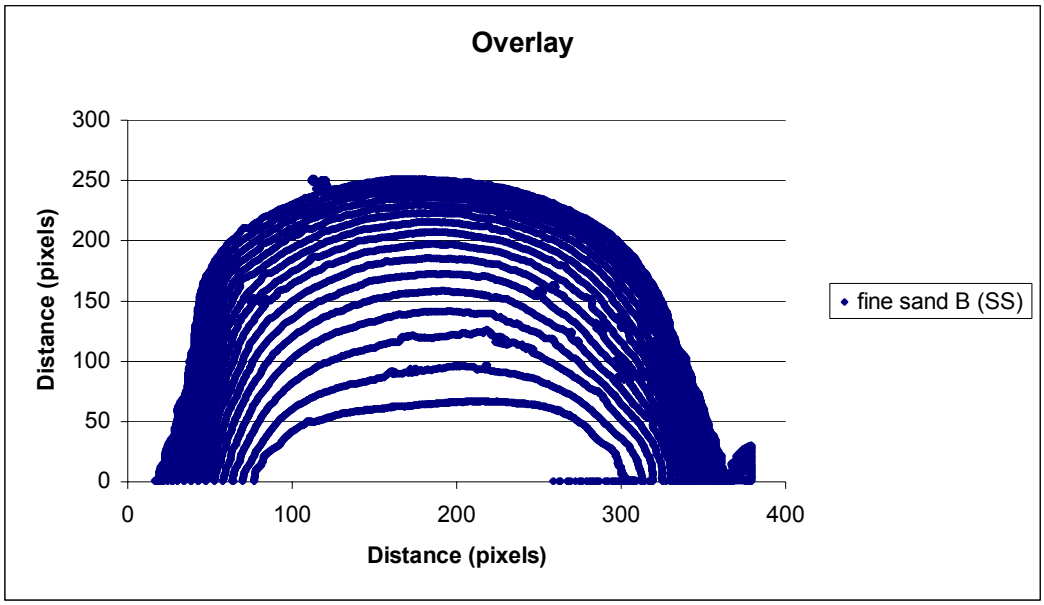

Fig 8a. Overlay of flow front (in Direction of Flow). The run consisted of fine sand material with a thickness of 10 cm over smooth substrate. The uncertainty for the high-resolution camera is ± 1 pixel and displayed 1 σ.

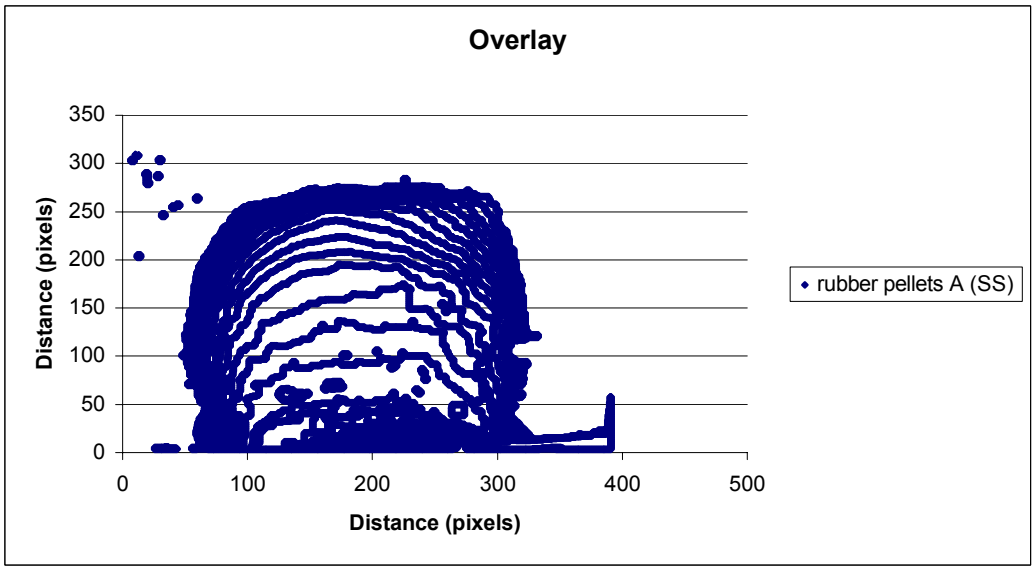

Fig 8b. Overlay of flow front (in Direction of Flow). The run consisted of rubber track material with a thickness of 10 cm over smooth substrate. The uncertainty for the high-resolution camera is ± 1 pixel and displayed 1 σ.

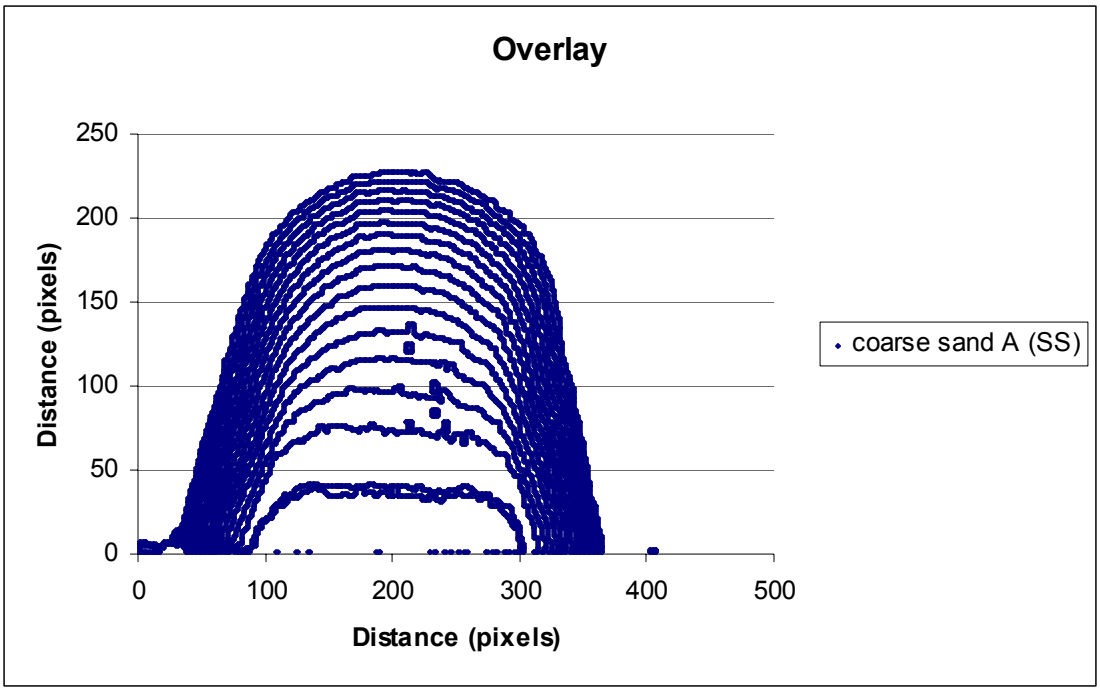

Fig 8c. Overlay of flow front (in Direction of Flow). The run consisted of coarse sand material with a thickness of 10 cm over smooth substrate. The uncertainty for the high-resolution camera is ± 1 pixel and displayed 1 σ.

The following graphs were created using the rough substrate. Figure 9 shows the averaged mean velocity of the flow materials over the rough substrate. The results show that all three materials slowed toward the contact with the substrate. Note the rubber track material is still the slowest material with nearly zero velocity. The coarse and fine sand significantly slowed, but maintained approximately the same velocity. Also the coarse and fine sand dramatically increase their velocities at the contact with the rough substrate while the track material continues to go even slower.

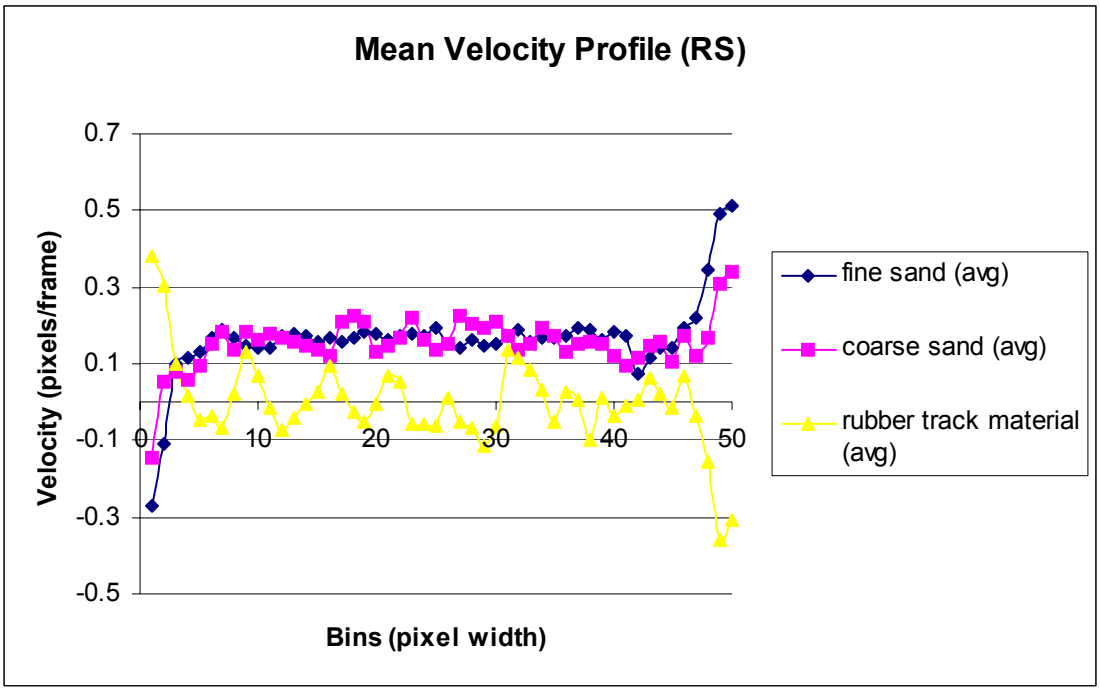

Fig 9. Flow Direction Mean Velocity for the viewing area of the fast-camera on a rough substrate. The total distance from the top of flow located at (0 bins), to the bottom of flow located at (50 bins) is 0.5 cm. Each bin is 5 pixels wide. The fifty bins are parallel to slope surface, which is at an angle of 33°. Note that the velocity decreases slightly as the flow gets closer to the substrate. Also note that at the contact with the substrate at (50 bins) the coarse and fine sand exhibit extreme increases in velocities. Uncertainty is ± 1 pixel and displayed in 1 σ.

Figures 10a-c show the velocity of the flow fronts (in the direction of flow) for each material on the rough substrate.

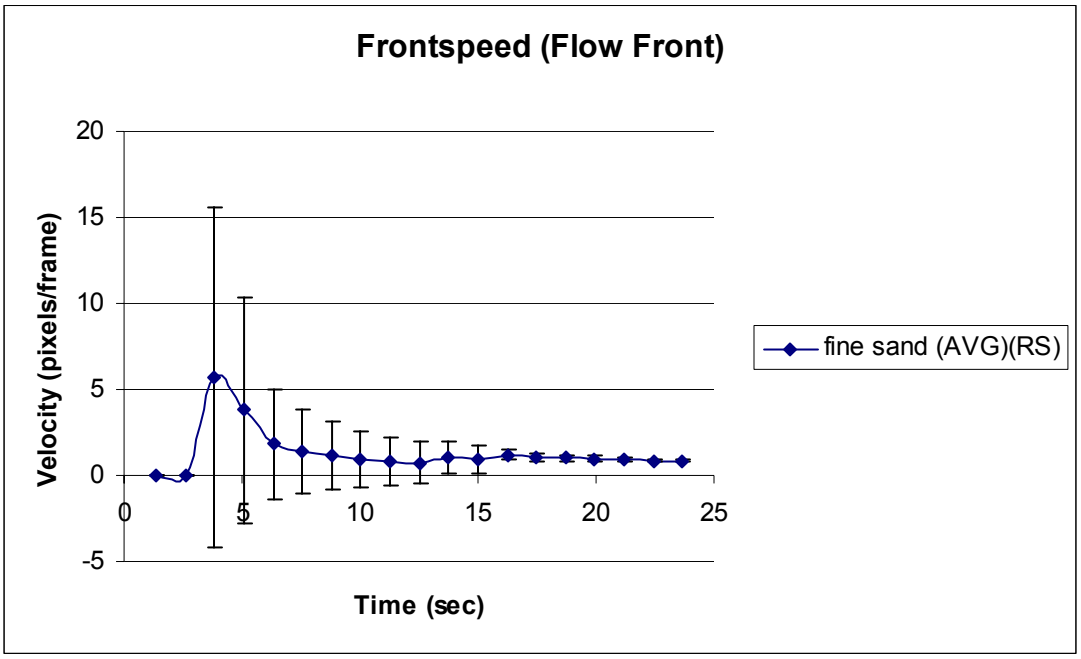

Fig 10a. Velocity of Flow Front (in Direction of Flow). The run consisted of fine sand material with a thickness of 10 cm over a rough substrate. The range for the high-resolution camera is ± 1 pixel and displayed 1 σ.

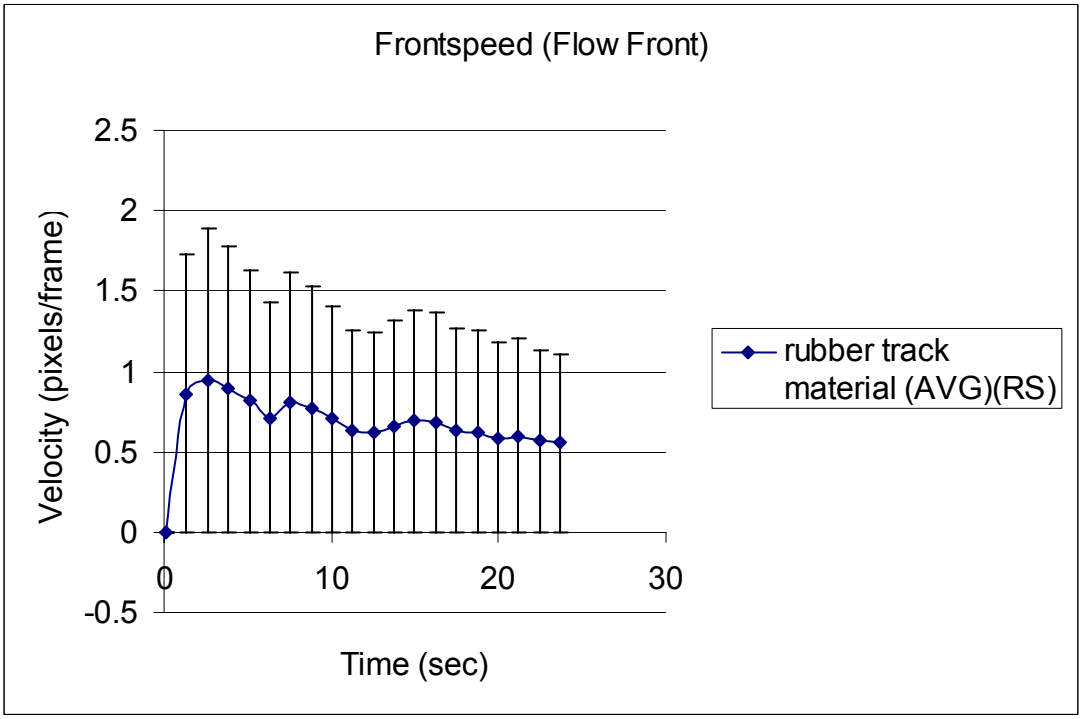

Fig 10b. Velocity of Flow Front (in Direction of Flow). The run consisted of rubber track material with a thickness of 10 cm over a rough substrate. The range for the high-resolution camera is ± 1 pixel and displayed 1 σ.

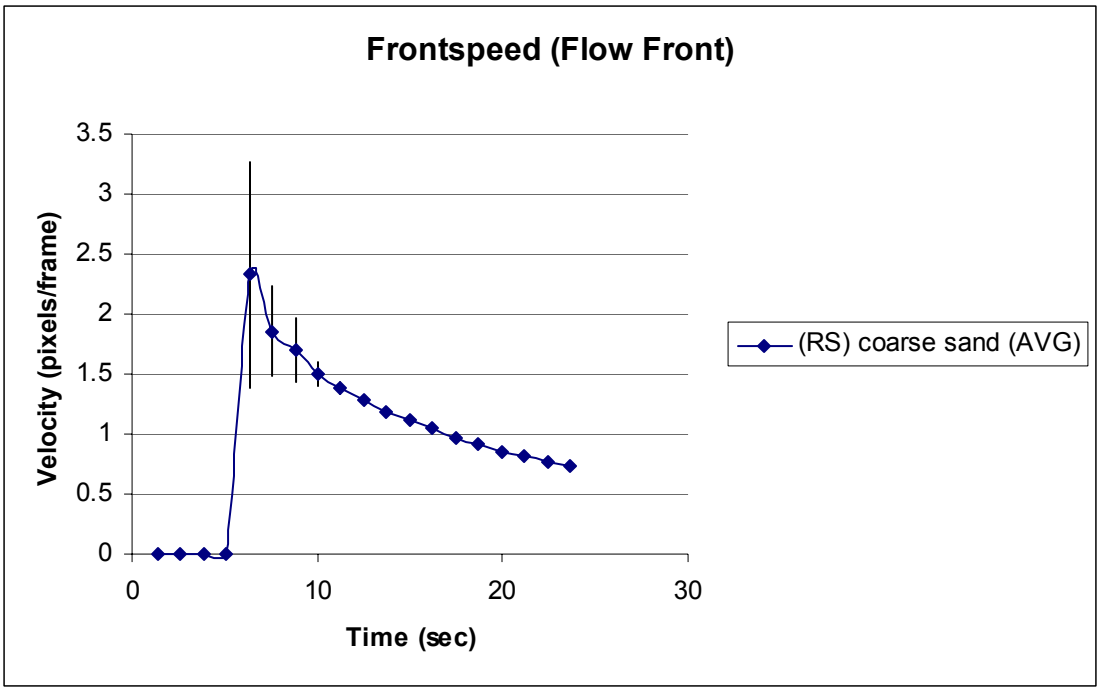

Fig 10c. Velocity of Flow Front (in Direction of Flow). The run consisted of coarse sand material with a thickness of 10 cm over a rough substrate. The range for the high-resolution camera is ± 1 pixel and displayed 1 σ.

Figures 11a-b show distance vs. time plots of the front center of flow of each material on the rough substrate.

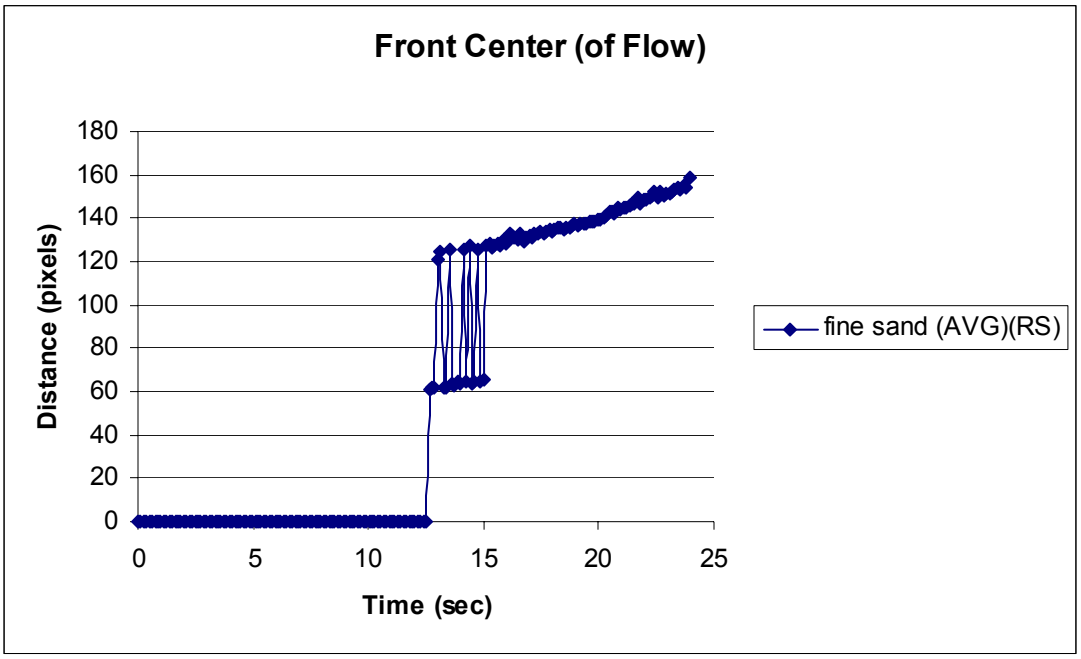

Fig 11a. Velocity of Front center of flow Front (in Direction of Flow). The run consisted of fine sand material with a thickness of 10 cm over a rough substrate. The uncertainty for the high-resolution camera is ± 1 pixel and displayed 1 σ. The particle tracking software had difficulty tracking most of the fine sand experiment for all three runs, which resulted in loss of data.

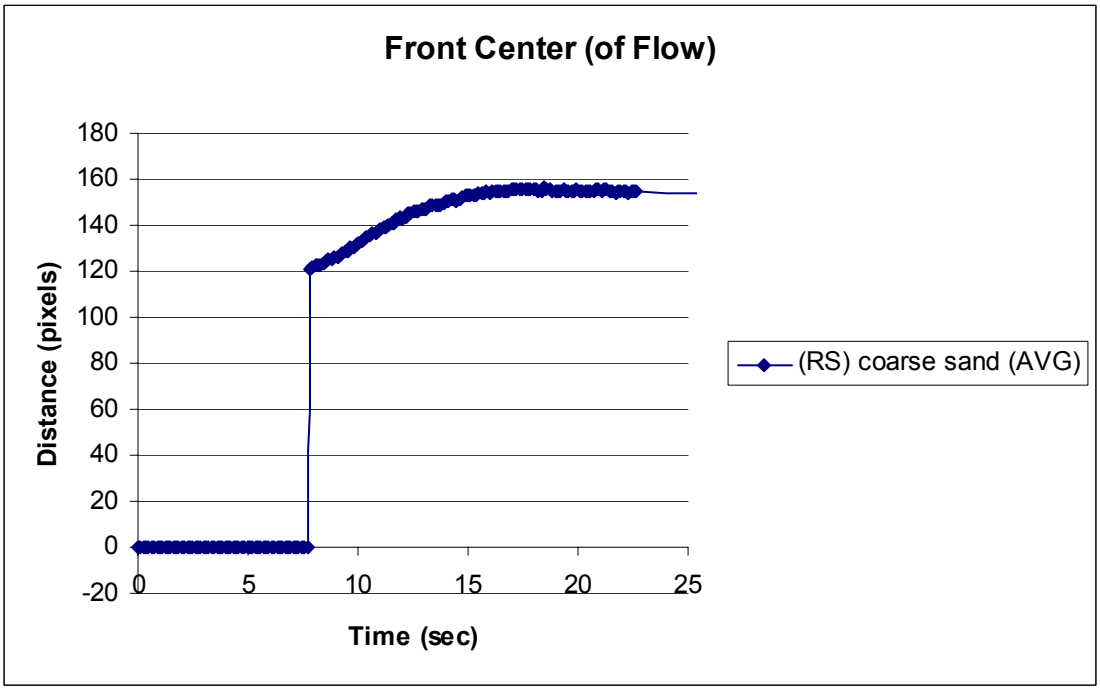

Fig 11b. Velocity of Front center of flow Front (in Direction of Flow). The run consisted of coarse sand material with a thickness of 10 cm over a rough substrate. The uncertainty for the high-resolution camera is ± 1 pixel and displayed 1 σ. The particle tracking software had difficulty tracking the first part of the coarse sand experiment for all three runs, which resulted in loss of data at the beginning.

Figures 12a-c show the front area of flow for all materials on the rough substrate.

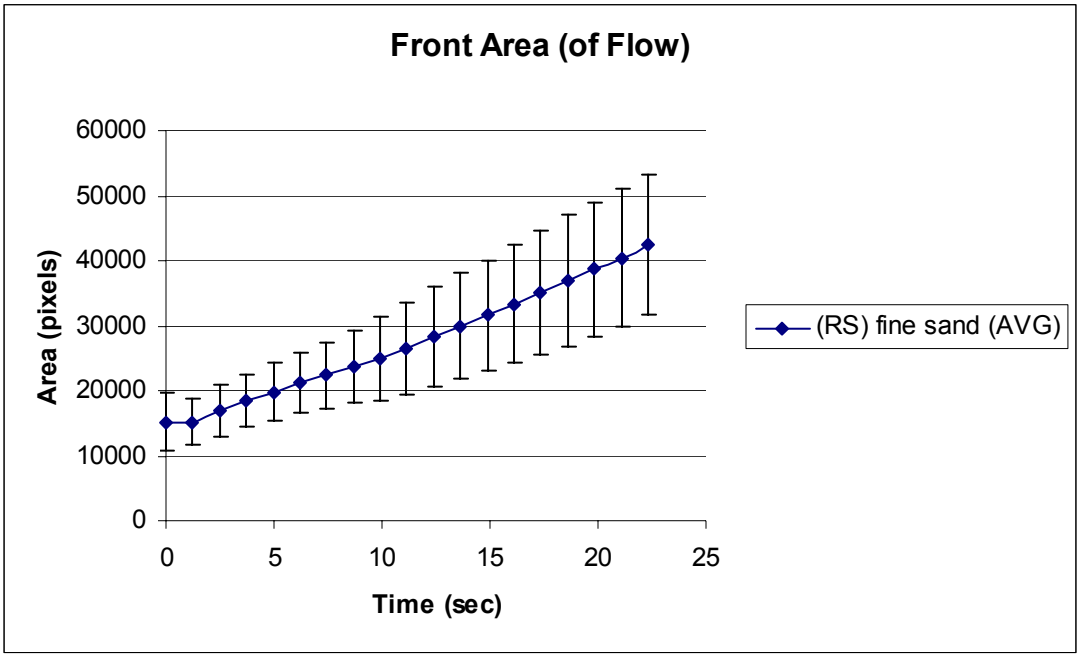

Fig 12a. The Front area of flow Front (in Direction of Flow). The run consisted of fine sand material with a thickness of 10 cm over a rough substrate. The range for the high-resolution camera is ± 1 pixel and displayed 1 σ. Note the almost linear slope.

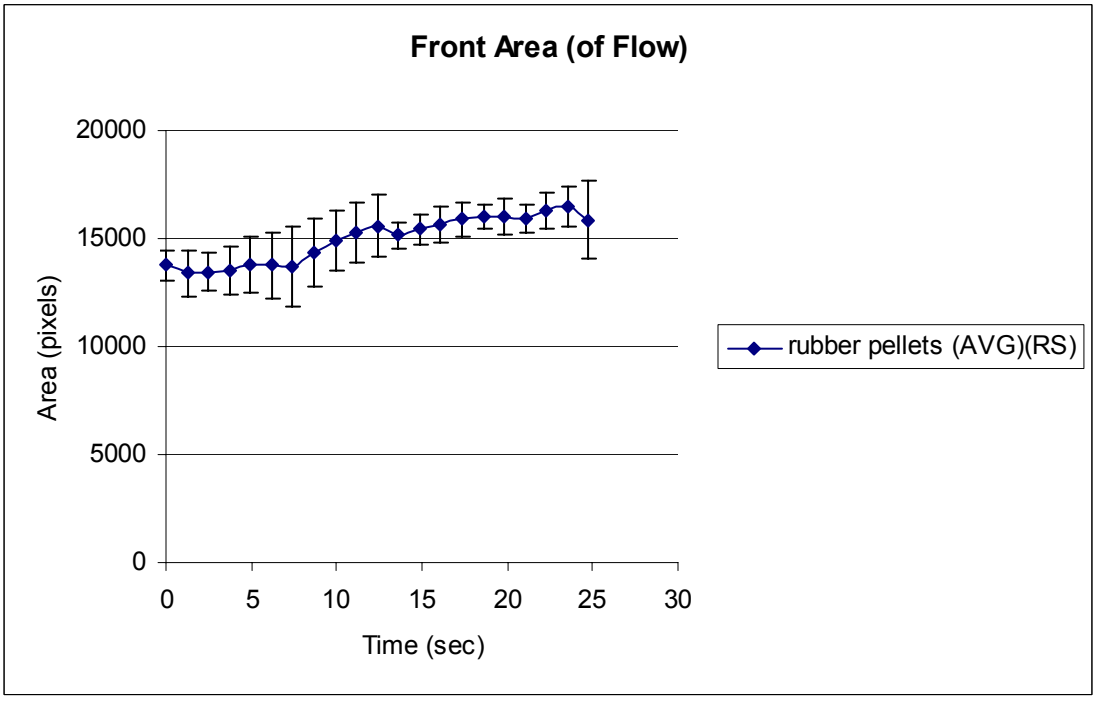

Fig 12b. The Front area of flow Front (in Direction of Flow). The run consisted of rubber track material with a thickness of 10 cm over a rough substrate. The range for the high-resolution camera is ± 1 pixel and displayed 1 σ.

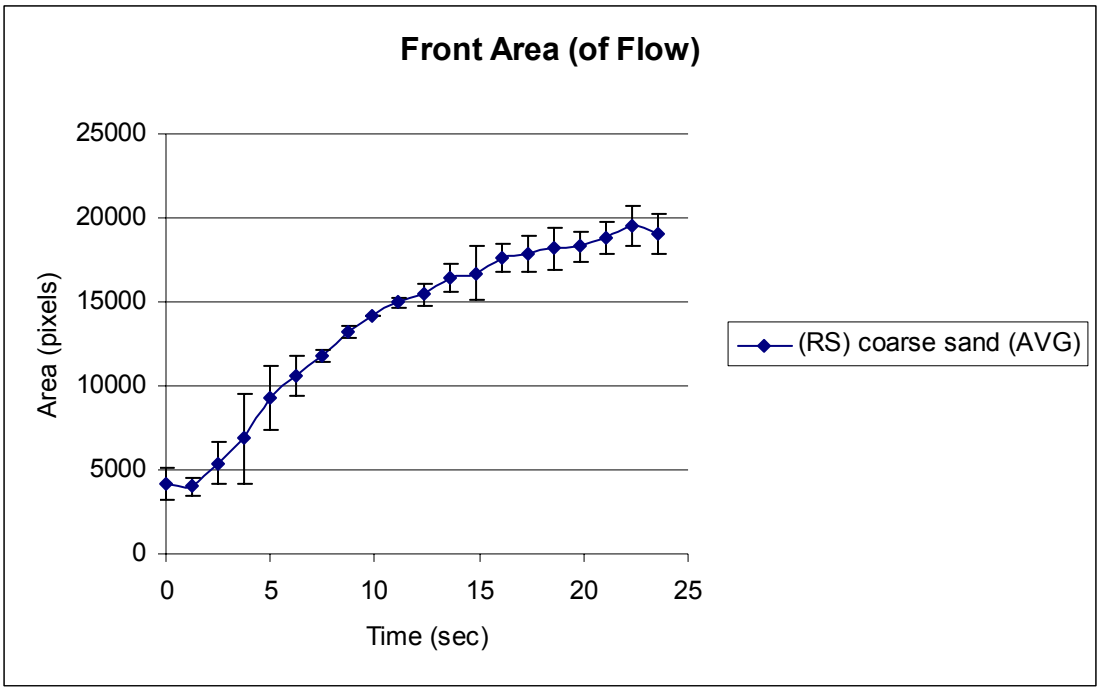

Fig 12c. The Front area of flow Front (in Direction of Flow). The run consisted of coarse sand material with a thickness of 10 cm over a rough substrate. The range for the high-resolution camera is ± 1 pixel and displayed 1 σ.

Figures 13a-c show position overlays of each material on the rough substrate.

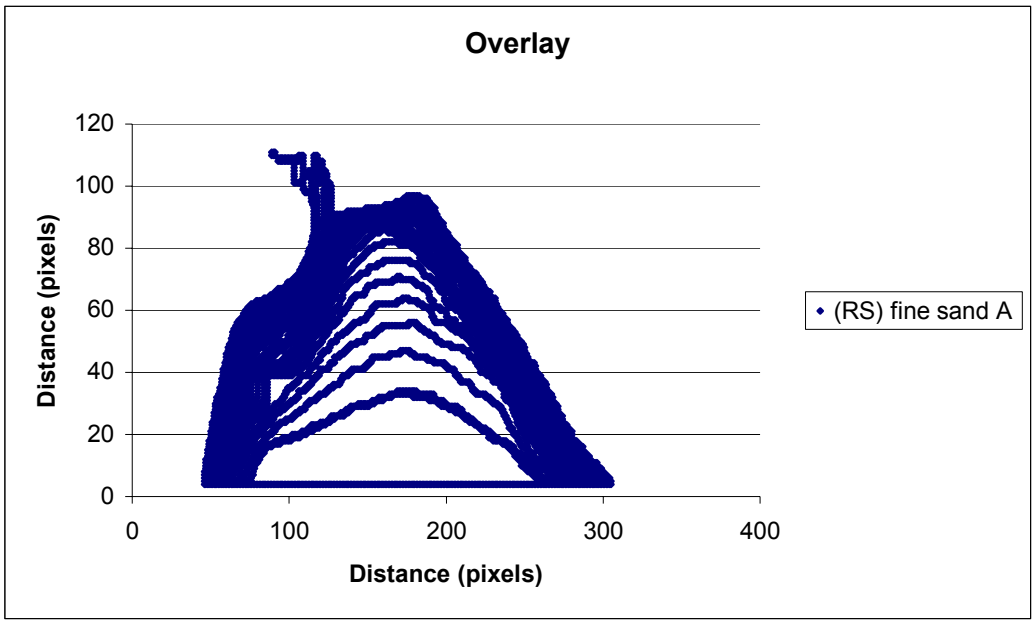

Fig 13a. Overlay of flow front (in Direction of Flow). The run consisted of fine sand material with a thickness of 10 cm over a rough substrate. The uncertainty for the high-resolution camera is ± 1 pixel and displayed 1 σ.

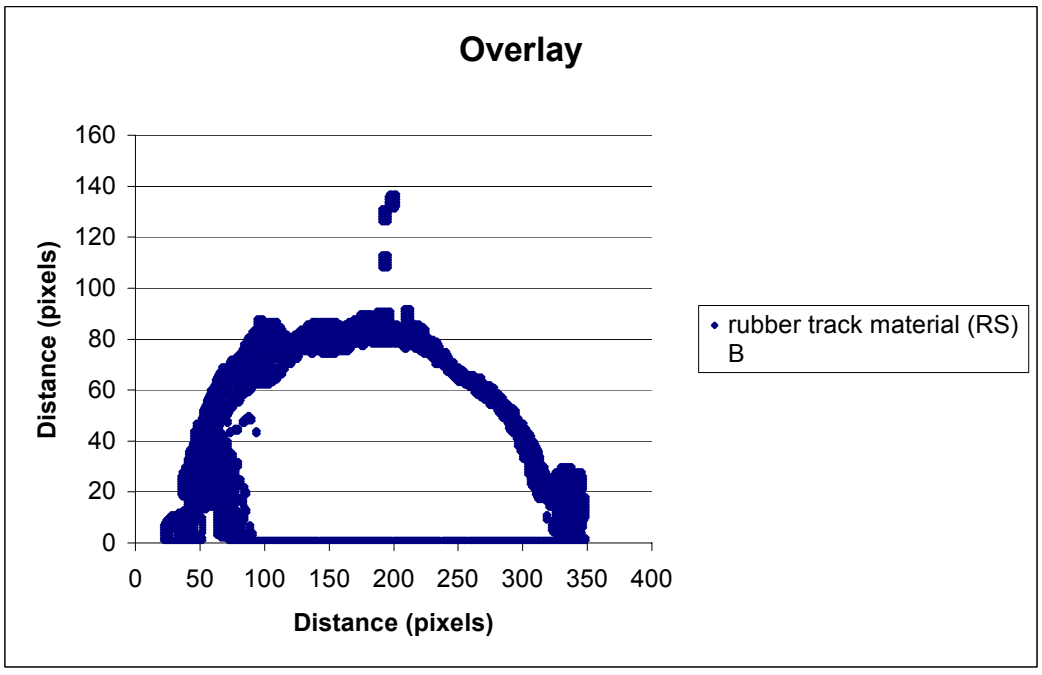

Fig 13b. Overlay of flow front (in Direction of Flow). The run consisted of rubber track material with a thickness of 10 cm over a rough substrate. The uncertainty for the high-resolution camera is ± 1 pixel and displayed 1 σ.

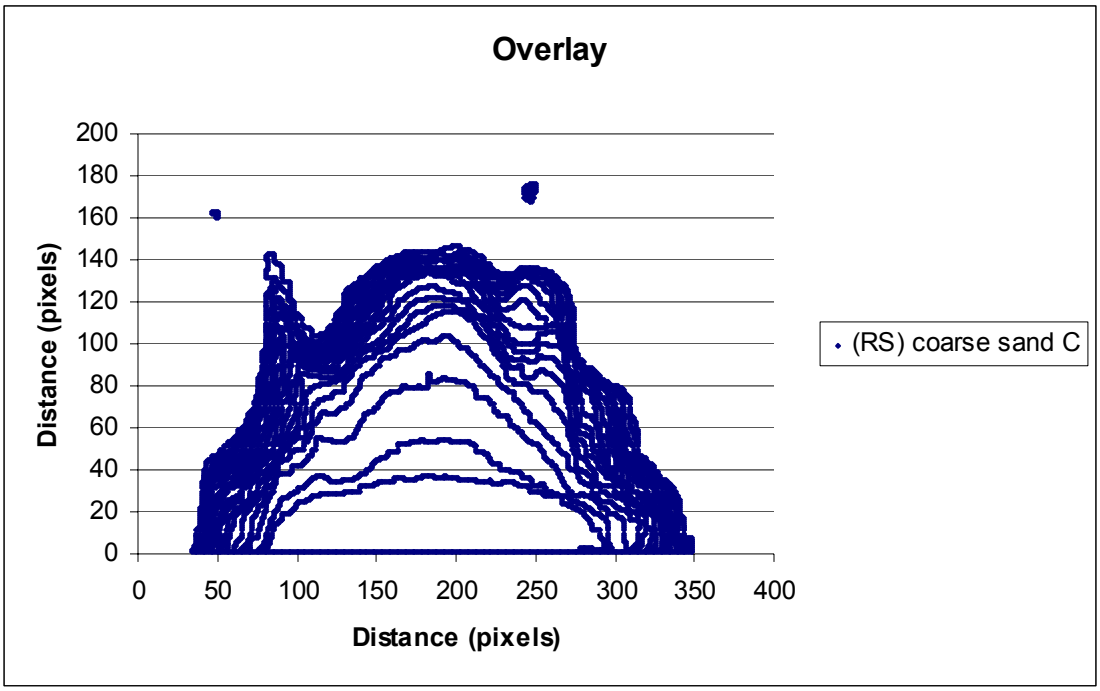

Fig 13c. Overlay of flow front (in Direction of Flow). The run consisted of coarse sand material with a thickness of 10 cm over a rough substrate. The uncertainty for the high-resolution camera is ± 1 pixel and displayed 1 σ.

The following graphs were created to compare the experiments with different substrates. Figure 14 shows the mean velocity profiles for all materials on both substrates.

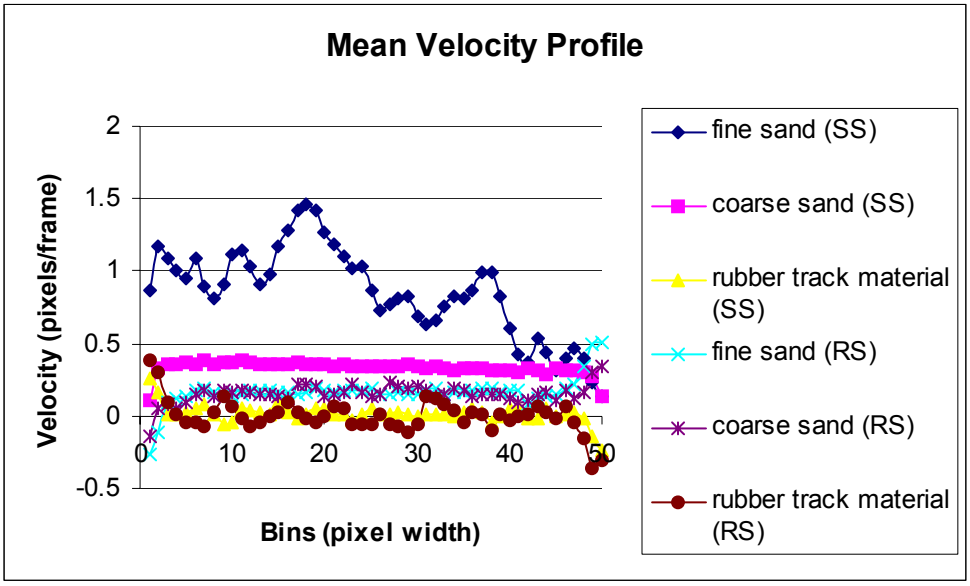

Fig 14. Flow Direction Mean Velocity for the viewing area of the fast-camera of both substrates. The total distance from the top of flow located at (0 bins), to the bottom of flow located at (50 bins) is 0.5 cm. Each bin is 5 pixels wide. The fifty bins are parallel to slope surface, which is at an angle of 33°. Note that the velocity decreases, as the flow gets closer to the substrate. Also note at the contact with the rough substrate at (50 bins) of the coarse and fine sand exhibit extreme increase in velocities. Uncertainty is ± 1 pixel and displayed in 1 σ.

Figure 15 shows the front-speed of all materials on both substrates.

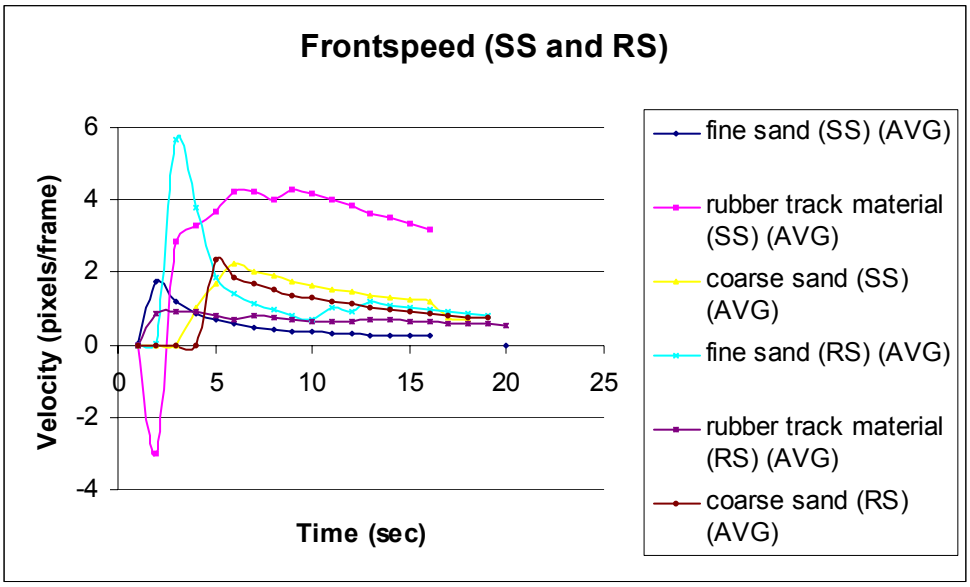

Fig 15. Velocity of Flow Front (in Direction of Flow). The run consisted of all materials over smooth and rough substrate with a thickness of 10 cm.

Figure 16 shows the front area (of flow front) for all materials on both substrates.

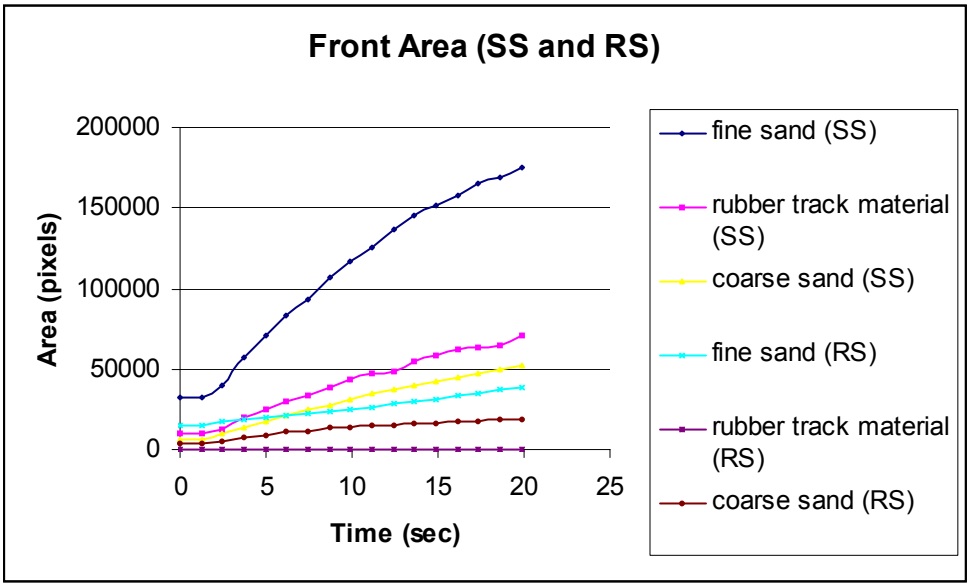

Fig 16. The Front area of flow Front (in Direction of Flow). The run consisted of all materials with a thickness of 10 cm over both substrates.

Figure 17 shows the front center of all materials on both substrates.

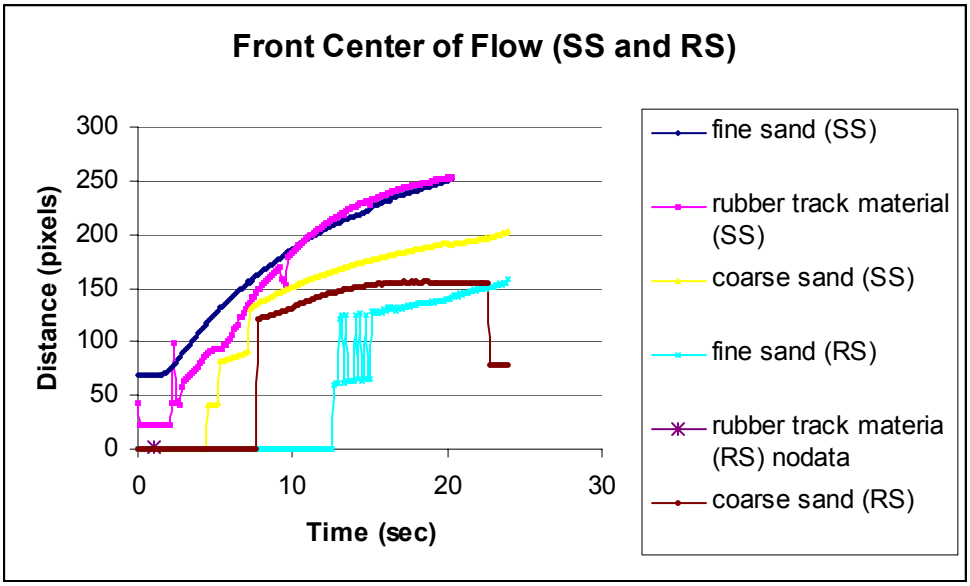

Fig 17. Velocity of Front center of flow Front (in Direction of Flow). The run consisted of all materials with a thickness of 10 cm over both substrates. The particle tracking software had difficulty tracking some of the materials, which resulted in loss of data.

IV. Discussion of Results

The mean velocity profiles were compiled from data obtained from the fast-camera. This data came from video recordings of the interactions at the substrate contact for both the smooth and rough surfaces. Both showed a decrease in velocity as the material came into contact with the substrate. In general, the material on the smooth surface had higher velocities than on the rough surface.

On the smooth substrate the fine sand was the fastest material, while the coarse sand had a velocity approximately three times slower. The rubber track material was the slowest with nearly zero velocity.

The materials observed on the rough surface showed a nearly constant speed. However, on average these materials were six times slower than on the smooth substrate. Once again the fine and coarse sand were the fastest materials, with a very slow velocity just above zero. The rubber track material was the slowest with nearly zero velocity. At the substrate contact the fine and coarse sand exhibited a sharp increase in velocity. This increase takes the material from 0.3 pixels/frame to approximately 0.5 pixels/frame. I attribute this increase in velocity to stick-slip of the material at the contact with the substrate.

The flow front velocity graphs were created from video using the high-resolution camera. This data also shows that the material on the smooth substrate had higher velocities than on the rough substrate.

On the smooth substrate the rubber track material at the top of the flow moved the fastest, while the coarse sand moved the slowest. This could be due to the mass of the materials used, so that the heaviest materials would produce slower velocities and

acceleration (The force is constant whereas the mass and accelerations vary). Also the fine and coarse sand show an exponential decrease in flow velocity. The track material is the fastest at the top of the flow, but the slowest at the contact with the substrate. This could be a factor of the energy dissipation abilities of the material. The rubber allows a lower dissipation rate, more elastic collisions. While the sand material has a higher dissipation rate causing more inelastic collisions.

The flow front profiles for the rough substrate show the fine sand had the highest velocities, while the rubber track material was the slowest. The increase in frictional character at the substrate causes the fine sand to flow easier due to the increase in particle contacts. The coarse sand maintains the same velocity regardless of substrate. This is probably due to the larger particle sizes of the coarse sand (the change in friction doesn't affect it as much).

The front area data was also produced from video taken from the high-resolution-camera. This data shows a near linear trend in area with time.

On the smooth substrate the fine sand covered the most area, with the coarse sand covering the least. On the rough substrate the fine sand again covered the most area, while the rubber track material covered the least. This may be attributed to the speed of the materials. The faster the material, the farther it will travel and cover more area. The front flow velocity profiles for the sand materials also showed an exponential decrease in velocity. The linear increase in area could be related to the exponential decrease. As the material covers new area, more surface contacts are created, thus increasing the amount of friction of the substrate; therefore, slowing down the material.

The overlay plots show the flow pattern of the material in time. On the smooth substrate the fine and coarse sand create a parabolic shape, while the rubber track material is semi-square. At the top of the flow the fine sand and track material run out about the same distances ~250 pixels. The coarse sand runs out a shorter distance of about 200 pixels. The rough substrate plots show the coarse sand runs out ~140 pixels, while the rubber track material travels about 90 pixels. The rough substrate patterns show more finger-like morphologies that mimic the topography of the wire mesh.

The individual grain sizes might cause more or less friction depending on the amount of contacts with other particles. Because the collisions of the sand material are inelastic, the fine sand (material with the most contacts) could translate more energy.

V. Suggestions for Future Work

Future experiments will include use of a laser sheet that will measure the distinct geomorphic features. The laser sheet was supposed to be used in the collection of this data, but we were unable to complete the computer programming associated with its use. The laser sheet projects a line across the deposited flow, at low angle and is deflected as a function of flow height. It will be used to measure shape data; flow width, spacing and height between ridges.

Other suggestions include the introduction of a high-resolution/fast camera that can view the entire width of the slope area. By capturing this on film, better observations/understandings of shear zones could be incorporated in the study.

Obstacles can be emplaced in the run-out area to observe the flow character as it comes in contact with the obstacles. Longer run times can be done to better study the velocities and accelerations of the material.

VI. Conclusion

Both substrates show different morphologies associated with them. The smooth substrate created parabolic flow shapes, while the rough substrate created semi-parabolic morphologies. These substrates created different shape patterns. In the case of the smooth surface, it resembles the Blackhawk type morphology.

The mechanics of each material changed depending on the substrate used. Each substrate produced different frictional character, which changed the velocity, distance and shape of each flow. The ability of the frictional character of the substrate to change the flow mechanics of material depends on the type of material used. The smooth surface showed the rubber track material had the highest velocity, which may be dependant on mass. The rough surface showed the fine sand had the highest velocity. I believe this is due to the smaller grain sizes along with the increase in frictional character at the substrate. The increase in particle contacts with the substrate allows the fine sand at the top of the flow to overtake the sand at the bottom, which creates faster flow velocities.

On the smooth substrate the fine sand covered the most area, with the coarse sand covering the least. On the rough substrate the fine sand again covered the most area, while the rubber track material covered the least. This may be attributed to the speed of the materials. The faster the material, the farther it will travel and cover more area.

By the observations of these materials under these specific conditions, I believe it

upholds the hypothesis that the substrate (coefficient of friction) is a critical parameter in the flow mechanics (as measured by velocity and distance) of dry granular landslides.

VII. Acknowledgements

I would like to thank my advisor Dr. Julio Friedmann for his guidance in this thesis project. I would also like to thank Dr. Wolfgang Losert and his graduate students for their time and knowledge in helping me understand the computer programming and laboratory equipment. Thanks to Mr. Don Martin for his assistance in designing and building the rock-avalanche apparatus. I would also like to thank Dr. Bhakti Petigara for her unconditional help during this thesis process.

VIII. Summary

Rock avalanches are large events that can cause catastrophic damage. A better understanding of the flow mechanics of rock avalanches can, in turn, help in efforts to minimize the destruction caused by these complicated landslides.

By simulating rock avalanches on a scaled-down model apparatus, flow character and morphology can be observed. Morphology of rock avalanches seems to be influenced by substrate as seen in Blackhawk and Sherman Glacier rock avalanches. In this study, the hypothesis that the substrate (coefficient of friction) is a critical parameter in the flow mechanics (as measured by velocity and distance) of dry granular landslides seems to be upheld.

In this study, two different substrates were used (smooth and rough) along with three different flow materials, to determine the importance of the coefficient of friction. It was shown at the base of the flow of the smooth surface, the smallest material (fine sand) had the highest velocity. At the top of the flow of the smooth surface, the lighter material (rubber track) had higher velocity and longer run-out. It was shown at the base of the flow of the rough surface, that all material slowed down significantly due to the increased friction. At the top of the flow of the rough surface the smallest material (fine sand) had the highest velocity and covered the largest area. The overall morphologies of these dry granular materials have parabolic shapes similar to that of the Blackhawk type rock-avalanches. It was shown that both substrates created different flow character.

IX. Works Cited

Bell, F.G. and Maud, R.R. (1999). Landslides Associated with the Colluvial Soils Overlying the Natal Group in the Greater Durban Region of Natal, South Africa. *Environmental Geology*. **39** (9), 1029-1038.

Campbell, C.S., Cleary, P.W., and Hopkins, M. (1995). Large-scale Landslide Simulations: Global Deformation, Velocities and Basal Shearing. *Journal of Geophysical Research*. **100** (B5), 8267-8283.

Challinor, J., (1978). A Dictionary of Geology 5th Ed. *Cardiff: University of Wales Press.*

Dai, F.C., Lee, C.F., Li, J., and Xu, Z.W. (2001). Assessment of Landslide Susceptibility on the Natural Terrain of Lantau Island, Hong Kong. *Environmental Geology*. **40** (3), 381-391.

Dutch, S., (1999). http://www.uwgb.edu/dutchs/202OVHDS/masswast.htm. *University Of Wisconsin-Green Bay.*

Erismann, T. H., (1979). Mechanics of Large Landslides: *Rock Mechanics*. **12**, 5-46.

Finlay, P.J., Mostyn, G.R., and Fell, R. (1999). Landslide Risk Assessment: Prediction of Travel Distance. *Can. Geotech. J*. **36**, 556-562.

Friedmann, J. (1997). Rock-Avalanche Elements Of The Shadow Valley Basin, Eastern Mojave Dessert, California: Processes And Problems. *Journal of Sedimentary Research.* **67** (5), 792-804.

Heim, A. (1882). Der Bergsturz von Elm. *Geol. Gesell. Zeitschr*., **34**, 74-115.

Hsu, J. (1975). Catastrophic Debris Streams (Sturzstroms) Generated by Rockfalls. *Geological Society of America Bulletin*. **86**, 129-140.

Keefer, D.K. (1984). Rock Avalanches Caused by Earthquakes: Source Characteristics. *Science*. **223**, 1288-1289.

Kent, P. E., (1966). The Transport Mechanisms of Catastrophic Rock Falls. *Journal of Geology*., **74**, 79-83.

Legros, F., Cantagrel, J-M., and Devouard, B. (2000). Pseudotachylyte (Frictionite) at the Base of the Arequipa Volcanic Landslide Deposit (Peru): Implications for Emplacement Mechanisms. *The Journal of Geology*. **108**, 601-611.

Losert, W. (2000). Particle Dynamics in Sheared Granular Matter. *Physical Review Letters*. **85** (7), 1428-1431.

Mullin, T. (2002). Mixing and Demixing. *Science*. **295**, 1851.

Poschel, T., Saluena, C., and Schwager, T. (2001). Scaling Properties of Granular Materials. *Physical Review E*. 64, 011308-1-011308-4.

Schuster, R.L. and Krizek, R.J. ed. (1978). Landslides: Analysis and Control. National Academy of Sciences: Washington D.C.

Shreve, R. L., (1968). The Blackhawk Landslide, *Geol. Society of America* Spec. Paper **108**, 47.

Wu, T.H., and Abdel-Latif, M.A. (2000). Prediction and Mapping of Landslide Hazard. *Can. Geotech. J*. **37**, 781-795.

Yarnold, J. (1993). Rock-Avalanche Characteristics in dry climates and the Effect of Flow into lakes: Insights from mid-Tertiary Sedimentary Breccias Near Artillery Peak, Arizona. *Geological Society of America Bulletin*. **105**, 345-360.